

Structural Evolution from Metal-Organic Framework to Hybrids of Nitrogen-Doped Porous Carbon and Carbon Nanotube for Enhanced Oxygen Reduction Activity

Linjie Zhang, Xiuyun Wang, Ruihu Wang, and Maochun Hong

Chem. Mater., **Just Accepted Manuscript** • DOI: 10.1021/acs.chemmater.5b02708 • Publication Date (Web): 30 Oct 2015

Downloaded from <http://pubs.acs.org> on November 2, 2015

Just Accepted

“Just Accepted” manuscripts have been peer-reviewed and accepted for publication. They are posted online prior to technical editing, formatting for publication and author proofing. The American Chemical Society provides “Just Accepted” as a free service to the research community to expedite the dissemination of scientific material as soon as possible after acceptance. “Just Accepted” manuscripts appear in full in PDF format accompanied by an HTML abstract. “Just Accepted” manuscripts have been fully peer reviewed, but should not be considered the official version of record. They are accessible to all readers and citable by the Digital Object Identifier (DOI®). “Just Accepted” is an optional service offered to authors. Therefore, the “Just Accepted” Web site may not include all articles that will be published in the journal. After a manuscript is technically edited and formatted, it will be removed from the “Just Accepted” Web site and published as an ASAP article. Note that technical editing may introduce minor changes to the manuscript text and/or graphics which could affect content, and all legal disclaimers and ethical guidelines that apply to the journal pertain. ACS cannot be held responsible for errors or consequences arising from the use of information contained in these “Just Accepted” manuscripts.

Structural Evolution from Metal-Organic Framework to Hybrids of Nitrogen-Doped Porous Carbon and Carbon Nanotube for Enhanced Oxygen Reduction Activity

Linjie Zhang, Xiuyun Wang, Ruihu Wang* and Maochun Hong

State Key Laboratory of Structural Chemistry, Fujian Institute of Research on the Structure of Matter, Chinese Academy of Sciences, Fuzhou, 350002, PR China

KEYWORDS: *Metal-organic frameworks; Hybrid materials; Carbon nanotube; Doping; Oxygen reduction reaction*

ABSTRACT: A series of hybrids of nitrogen-doped graphitic porous carbon and carbon nanotube (NGPC/NCNTs) are readily prepared in a stepwise manner by using a typical metal-organic framework (MOF-5) and urea as the carbon and nitrogen precursors, and nickel as the graphitization catalyst, respectively. These NGPC/NCNTs hybrids have demonstrated prominent catalytic activities toward oxygen reduction reaction (ORR) in alkaline medium. Compared to the benchmark Pt/C catalyst, the optimized NGPC/NCNT-900 (annealed at 900 °C) exhibits superior catalytic activity, durability and methanol tolerance, which makes it one of the best ORR electrocatalysts derived from MOFs. The promising properties in NGPC/NCNT-900 are mainly attributed to synergistic contributions of its unique hybrid structure, rich nitrogen doping, high graphitic degree and large surface area. This attractive route for the preparation of NGPC/NCNTs holds promise for general use of a great number of available and yet rapidly growing MOFs in constructing high-performance carbon-based ORR electrocatalysts.

INTRODUCTION

Exploring cost-effective Pt-free electrocatalysts while maintaining the high performance as Pt is one of the most active and competitive fields for oxygen reduction reaction (ORR) in fuel cells.¹⁻³ In this context, heteroatom (N, S, B, P, Fe and Co etc.)-doped carbon-based materials have achieved striking performance in superseding of Pt-based catalysts.⁴⁻⁶ Despite the rapid progress, there still remains a multitude of deficiencies in the development of doped carbon (DC) electrocatalysts. On one hand, the traditional chemical vapor deposition (CVD) approach or plasma treatment for the synthesis of DCs usually involves harsh handling conditions and uncontrollable heteroatom doping. On the other hand, their ORR activities rarely out-compete Pt-based materials in term of the half-wave potential ($E_{1/2}$), even with a higher onset potential (E_o) or diffusion-limited current density (j_L).^{7, 8} Therefore, it is highly desirable but challenging to develop a facile strategy for controllable synthesis of DC electrocatalysts with enhanced ORR activity.

Metal-organic frameworks (MOFs) are constructed by organic linkers and metal ions/clusters, and are an attractive class of highly customizable porous crystalline materials with flexible tunability in compositions, structures and properties. In the last couple of years, MOFs have emerged as both promising precursors and templates for the synthesis of porous DCs due to their plentiful heteroatoms other than carbon and readily self-sacrificial nature.⁹⁻¹¹ Hitherto, various DCs have been directly cast from MOFs with the addition of heteroatom-containing organic molecules,¹²⁻¹⁴ and the influences of guest molecules and host MOFs on ORR

activities of MOF-derived DCs (MDCs) have been well studied, but the results are still unsatisfactory.¹⁵⁻¹⁸ Considering the accessible large surface area and high-density active sites inherited from parent MOFs and/or foreign agents, the most possible factor retarding the performance of MDCs may be their intrinsically poor electroconductive carbon skeletons, the majority of which are presented in disorder, namely, amorphous carbons. In contrast, most of doped-carbon nanotubes (CNTs), graphenes and carbon blacks show obviously higher ORR activities owing to their better electronic conductivity.¹⁹⁻²¹ Recently, it has been reported that DCs derived from CNTs- or graphene oxides-supported ZIF-8 exhibit substantially higher ORR activities than those derived from dissociative ZIF-8 particles due to their high and consecutive electronic conductivity.^{22, 23} Nevertheless, such strategy is lack of generality because of the diverse and complicated surface interactions between MOFs and electroconductive inorganic supports. In addition, the crystallization process of MOFs on such supports is uncontrollable. The improvement of electronic conductivity of individual MDC seems to be a more fundamental issue that should be resolved preferentially.

It is known that high electronic conductivity of carbon materials is closely correlated to their high crystallinity, i.e., high degree of graphitization, which can simultaneously enhance the electron transfer rate and the corrosion resistance. Although graphitization of MDCs can be somewhat induced during high temperature treatment of MOFs,²⁴⁻²⁶ the degree is very limited, and both the pore structure and carbon-heteroatom bonds can be seriously destroyed when the

temperature is too high. Encouragingly, amorphous carbon can be transformed into highly graphitic carbon under relative low temperature (< 1000 °C) in the presence of catalytic metals, such as Fe, Mn and Ni.^{27, 28} Both Su and Wang *et al.* successively proposed that highly graphitized carbons could be obtained through pyrolysis of Fe- or Co-based MOFs due to the catalytic graphitization of metal nanoparticles (NPs) in situ formed during pyrolysis of MOFs.^{15, 29} However, most of MOFs are not composed of such catalytic metal ions/clusters, thus hindering MDCs to perform to their maximum potential in ORR activities. In response, post-addition of catalytic metals into MOF-derived carbons could be a good alternative. Herein, we present a unique route for the efficient synthesis of highly graphitized porous carbons (GPCs) based on the well-known MOF-5 ([Zn₄O(BDC)₃], H₂BDC = benzene-1,4-dicarboxylate) with the aid of exotic Ni, subsequent nitridation using urea induces further structural evolution of GPCs, resulting in the formation of hybrids of nitrogen-doped graphitic porous carbon and carbon nanotube (NGPC/NCNTs). The representative product NGPC/NCNT-900 (the anneal temperature of urea@GPC being 900 °C) exhibits superior ORR activity than the benchmark Pt/C with a slightly higher $E_{1/2}$ in the alkaline medium, ranking it among the best ORR electrocatalysts derived from MOFs.

EXPERIMENTAL SECTION

Synthesis of NGPC/NCNT Hybrids. Pristine MOF-5 was synthesized according to literature method.³⁰ All anneal processes were conducted at a heating rate of 5 °C min⁻¹ under a stream of N₂ (0.5 s.c.c.m) after excluding air by flushing N₂ for 30 min. In the first step, the activated MOF-5 (2.0 g) was weighed in a ceramic boat and transferred into a quartz tube. The tube was sealed and placed inside a furnace, where the carbonization was performed at 550 °C for 1 h. After natural cooling to room temperature, the resulting black powders were washed by 1 M aqueous HCl solution and dried in vacuum, the product (referred to as C₅₅₀) was harvested in a 25% yield. In the second step, a given amount of C₅₅₀ and nickel formate (3 mmol g⁻¹ C₅₅₀, Alfa Aesar) in distilled water were stirred for 12 h, then vacuum-dried and pyrolyzed at 1000 °C for 3 h. The resulting material was hydrothermally etched in 10 M aqueous HCl solution containing 1.25 wt% H₂O₂ at 160 °C for 24 h to remove metal species. After rinse with 34 wt% HNO₃ for several hours, followed by a complete wash with water until the filtrate was neutral, the sample was dried in air (referred to as GPC). In the third step, a mixture of GPC and urea with mass ratio of 1:10 in distilled water was sonicated for 2 h, and followed by a vigorous stir at room temperature for 12 h. The resulting suspension was dried under vacuum at 60 °C, and then pyrolyzed at the target temperature (800, 900 and 1000 °C) for 3 h. The as-prepared samples are denoted as NGPC/NCNT-*x* (*x* represents the temperature). All carbon samples were activated under vacuum at 200 °C for 10 h before being used for electrochemical study.

For comparison, pristine undoped porous carbon (C-MOF-5) and non-catalytically graphitized nitrogen-doped porous carbon (NPC) were also synthesized by direct carbonization (900 °C for 3 h) of MOF-5 and MOF-5 extracted from a urea-saturated methanol solution, respectively.

Physical Characterizations. Scanning electron microscopy (SEM) was performed on a Hitachi SU8010. High-resolution transmission electron microscopy (HR-TEM) images were taken on an FEI Tecnai F20. The textural properties of the samples were measured on a Micromeritics ASAP 2020 using nitrogen sorption at 77 K. Powder X-ray diffraction (PXRD) was determined on a Rigaku MiniFlex 600 diffractometer with Cu K_α radiation. The patterns were obtained at a scan rate of 5° min⁻¹ with a step of 0.02°. X-ray photoelectron spectroscopy (XPS) was performed on a Thermo Scientific ESCALAB 250 spectrometer using an Al K_α source. High-resolution spectra were acquired with a 20 eV pass energy. The area of analysis was 700 × 300 μm in size, and each sample was analyzed at a 90° takeoff angle with a depth of 3–4 nm. Raman spectra were obtained using a Renishaw UV-1000 Photon Design spectrometer at 532 nm excitation focused through at 100 × microscope objective for a total interrogation spot size of ~ 1 μm. Thermogravimetric analysis (TGA) was carried out on a Netzsch STA449C from room temperature to 1000 °C with a heating rate of 5 °C min⁻¹ under a nitrogen flow. Fourier-transform infrared spectroscopy (FT-IR) was conducted on a Bruker VERTEX 70 with samples prepared as KBr pellets at wavenumbers ranging from 4000 to 400 cm⁻¹. Elemental analyses and determination of metal species were performed on vario MICRO elemental analyzer and Ultima 2 inductively coupled plasma optical emission spectrometer (ICP-OES), respectively.

Electrochemical Measurements. Rotating disc electrode (RDE) testing was conducted to evaluate ORR activity. 1 mg of catalyst was dispersed in 1 mL of isopropanol/water [25:75 (v/v)] ink containing 10 μL 5 wt% Nafion. 20 μL of the ink mixture was then deposited on a glassy carbon electrode ($\Phi = 5$ mm). Testing was conducted by sweeping the electrode potential from 0.1 to -1 V versus Ag/AgCl electrode (5 mV s⁻¹) in an oxygen-saturated 0.1 M aqueous KOH solution at room temperature. Electrode kinetic data were calculated according to the well-known Koutecky–Levich (K–L) equation:

$$1/j = 1/j_L + 1/j_K = 1/B\omega^{1/2} + 1/nFkC_0 \quad (1)$$

$$B = 0.62nFD_0^{2/3}v^{-1/6}C_0 \quad (2)$$

where j , j_L , j_K are the measured current density, the diffusion-limited current density and the kinetic current density, respectively; ω is the angular velocity of the rotating electrode, F is the Faraday constant (96,485 C mol⁻¹), D_0 is the diffusion coefficient of oxygen in 0.1 M KOH (1.9 × 10⁻⁵ cm² s⁻¹), v is the kinetic viscosity (0.01 cm² s⁻¹), and C_0 is the bulk concentration of oxygen (1.2 × 10⁻⁶ mol cm⁻³). The electron transfer numbers (n) and kinetic current densities (j_K) were extracted from the slopes and the intercepts of linear K–L plots, respectively.

The electron transfer numbers (n) as well as the HO₂⁻ intermediate production percentage (HO₂⁻%) can also be obtained from the rotating ring-disk electrode (RRDE) voltammograms using the following equations:

$$n = 4 \times I_d / (I_d + I_r/N) \quad (3)$$

$$HO_2^- \% = 200 \times I_r/N / (I_d + I_r/N) \quad (4)$$

here I_d and I_r are the disk current and ring current, respectively, and N is the current collection efficiency of the

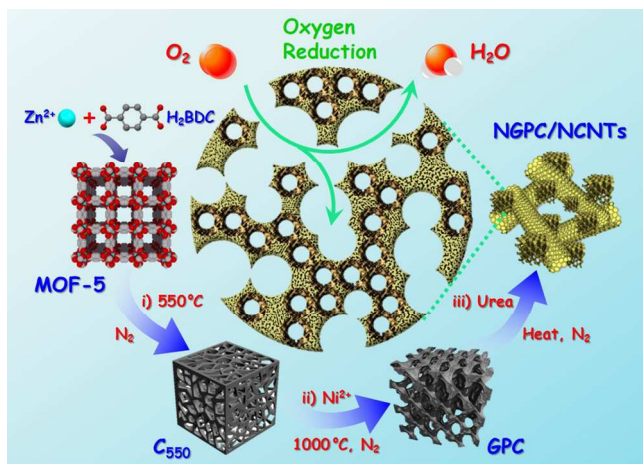


Figure 1. Schematic illustration of the stepwise structural evolution from MOF-5 to NGPC/NCNTs.

Pt ring (0.37). Chronoamperometric measurements were performed at a static cathodic potential and an electrode rotation speed of 1600 rpm in O₂-saturated 0.1 M KOH solution to investigate stability and possible poisoning effect of the catalysts.

RESULTS AND DISCUSSION

Synthesis and Characterizations of Electrocatalysts

The route for stepwise structural evolution from MOF-5 to NGPC/NCNTs is schematically shown in Figure 1. MOF-5 was readily available by the reaction of Zn²⁺ and benzene-1,4-dicarboxylic acid, subsequent carbonization at 500 °C, and followed by the removal of residual ZnO with aqueous HCl solution generated primary carbide C₅₅₀. Subsequently, Ni(II) salts were impregnated into C₅₅₀ and the mixture was catalytically graphitized at 1000 °C, GPCs were then obtained after the in situ formed Ni NPs were hydrothermally etched off. The GPCs were further nitrided with urea at 800, 900 and 1000 °C to give the nitrogen-doped products NGPC/NCNT-800, NGPC/NCNT-900 and NGPC/NCNT-1000, respectively.

The typical scanning electron microscopy (SEM) and transmission electron microscopy (TEM) images of MOF-5 precursor and the resultant various carbon samples are shown in Figure S1 and S2 (Supporting Information), respectively. The parent MOF-5 are uniform shuttle-like microplates with average length of ~1 μm, while both C₅₅₀ and GPCs are presented as non-uniform particulates, which comprise distinct hierarchical porous structures as a result of the removal of ZnO. Compared with C₅₅₀, GPCs show well-distinguished graphitized nanostructures, indicating the effective catalytic graphitization by Ni NPs. NGPC/NCNT-800, NGPC/NCNT-900 and NGPC/NCNT-1000 clearly show the same hybrid structure with heterogeneous morphologies of carbon particulates (CPs) and nanotubes. Representatively, the optimal NGPC/NCNT-900 is presented here in detail. As shown in Figure 2a and b, CPs generally appear as an irregular shape, their sizes range from tens to hundred nanometers, while CNTs show bamboo-like shape with open ends, and the length can be up to several micrometers. The selected-area electron diffraction (SAED) pattern shows four clear diffraction rings (inset in Figure 2b), which can be assignable to graphitic carbon. More importantly, one single CNT in the

hybrid can bridge several dissociative CPs to construct an interconnected three-dimensional (3D) conductive network (Figure 2a–c), which is highly favored for ORR. A close view of CPs further reveals the presence of many onion-like hollow carbons (marked as white dashed circles) as a result of the demetalation after the catalytic graphitization (Figure 2d). The corresponding high-resolution TEM (HR-TEM) images in Figure 2e and 2f show oriented multilayer graphite nanostructures on both the hollow carbon onions ($d_{002} = 0.3435$ nm) and the domains between them, respectively, indicating high graphitic degree of these CPs.³¹ Furthermore, CNTs appear with relatively uniform sizes in both diameter and bamboo joint distance (Figure 2g). Based on a specific CNT shown in Figure 2h, the outer diameter and joint length are measured to be ca. 30 and 20 nm, respectively. The corresponding magnified image at the walls and joints manifests the coaxially rolling thin graphene nanoshells ($d_{002} = 0.3423$ nm) and the cup-like joints preserving integrity along the *c*-axis (Figure 2i), which is beneficial to rapid electron transfer. The bamboo-like joints represent a typical morphological feature of N-doped CNTs,³² which is further verified by high-angle annular dark-field scanning transmission electron microscopy (HAADF-STEM) and the elemental mapping (Figure 2j–l), where a uniform nitrogen distribution is observed on both CP and CNT, indicating nitrogen atoms are well hybridized into the graphitic carbon structure. Compared to NGPC/NCNTs, both nitrogen-undoped C-MOF-5 and nitrogen-doped NPC that straightforwardly prepared from pristine MOF-5 are presented as irregular porous particulates, which are the same as CPs but only show a few undistinguishable graphene sheets at the margin (Figure S1 and S2).

To further clarify the bonding configuration of nitrogen dopants in NGPC/NCNTs and NPC, X-ray photoelectron spectroscopy (XPS) measurements were conducted. The survey spectra confirm that all samples show a predominant peak at 284.7 eV corresponding to C 1s. The minor peaks at 399.6 and 531.8 eV can be assigned to N 1s and O 1s (probably due to the physically adsorbed oxygen species, e.g., H₂O and CO₂),³³ respectively, suggesting their complete conversion to nitrogen-doped carbonaceous materials (Figure S3). In C 1s XPS spectra, the appearance of asymmetric tails at high binding energies with deconvoluted peaks at 286.5 eV (C–N/C–O) and 287.6 eV (C=N/C=O) further verifies the successful nitrogen doping of NGPC/NCNTs and NPC (Figure 3a and S4a).³⁴ The high-resolution XPS spectra of N 1s are deconvoluted into four sub-peaks including pyridinic-N (N1, 398.4 eV), pyrrolic-N (N2, 400 eV), graphitic-N (N3, 401.1 ± 0.1 eV) and pyridine-N-oxide (N4, 402.4 ± 0.2 eV) (Figure 3a and S4b).^{35, 36} The summarized data regarding these nitrogen dopants are shown in Table S1. A high nitrogen doping level of 7.53 wt% is achieved in NPC. Whereas for NGPC/NCNTs, as the nitridation temperature increases, a gradual decrease in the total nitrogen content from NGPC/NCNT-800 (5.89 wt%) to NGPC/NCNT-900 (5.04 wt%) to NGPC/NCNT-1000 (2.56 wt%) is observed owing to the continuous escape of nitrogen based on the cleavage of C–N/C=N.³⁷ Meanwhile, there is no detectable Ni signals (ca. 850–870 eV) in the surface layers (up to 3–4 nm) of NGPC/NCNTs. However, the determination of metal contents in GPCs by inductively coupled plasma optical emission spectrometry (ICP-OES) still discloses the presence of a trace of Ni (0.46 wt%), implying the residual Ni NPs are well enclosed by the thick graphitic carbon layers,

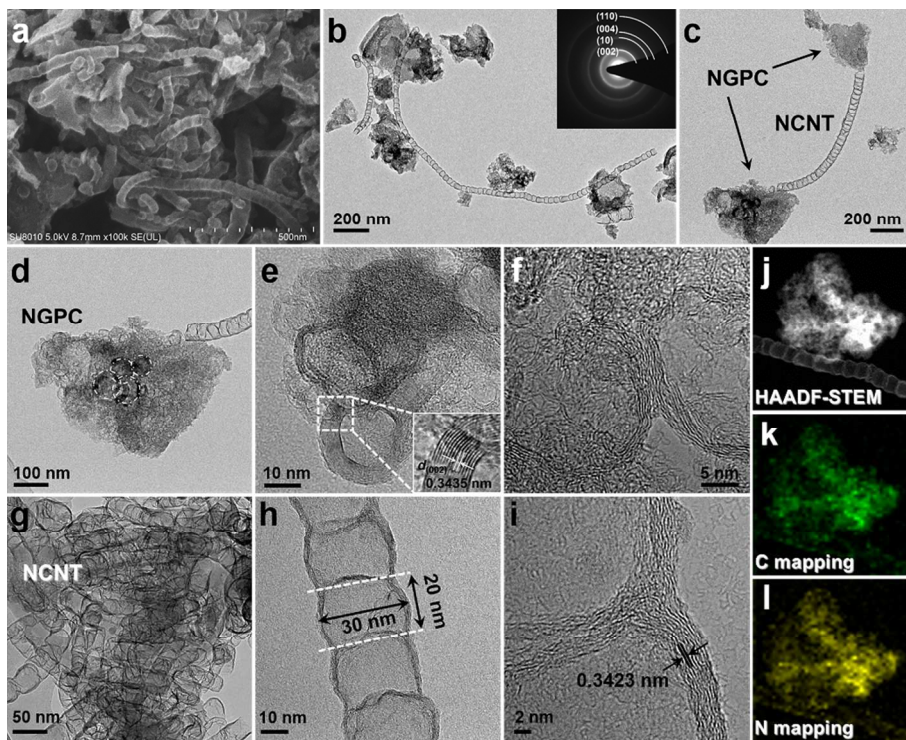


Figure 2. Representative (a) SEM and (b, c) TEM images of NGPC/NCNT-900, inset in (b) is the corresponding selected-area electron diffraction (SAED) pattern; (d–f) and (g–i) are the typical TEM and HR-TEM images of NGPCs and NCNTs in NGPC/NCNT-900, respectively; (j–l) HAADF-STEM and elemental mapping images of NGPC/NCNT-900.

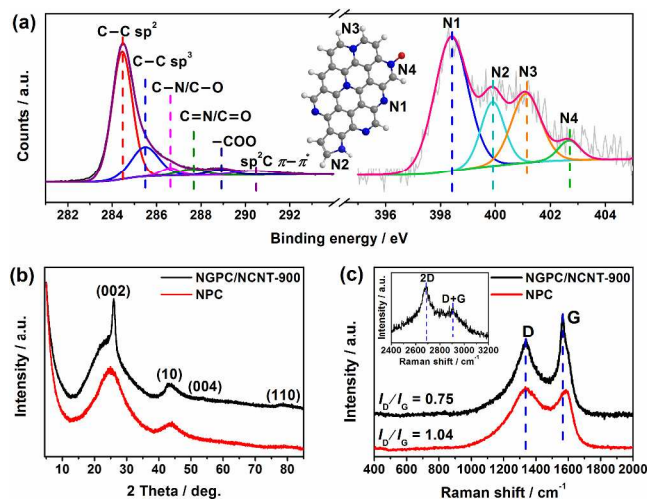


Figure 3. (a) High-resolution C 1s and N 1s XPS spectra of NGPC/NCNT-900 (inset shows the four configurations of nitrogen dopants); (b) PXRD patterns and (c) Raman spectra of NGPC/NCNT-900 and NPC (inset in (c) is the second-order spectrum of NGPC/NCNT-900).

which can be inferred from the formation of hollow carbon-onions in NGPCs.

In order to have a better knowledge of NGPC/NCNTs, various other characterizations were conducted. Powder X-ray diffraction (PXRD) patterns of NGPC/NCNTs and NPC are shown in Figure 3b and S5. Four peaks at 26, 43, 54 and 77° are found for NGPC/NCNTs, which can be indexed to the (002), (100)/(101), (004) and (110) reflections of graphitic carbon (JCPDS No. 75-1621), respectively. The sharp (002)

peak in PXRD patterns of NGPC/NCNTs clearly reveals their high graphitic degree.³⁸ For NPC, there are two broad diffraction peaks at 25 and 44°, attesting its amorphous carbon nature. This can be further discerned by the intensity ratio (I_D/I_G) of the peaks roughly at 1340 cm^{-1} (D band) and 1560 cm^{-1} (G band) in their Raman spectra (Figure 3c and S6).³⁹ As the nitridation temperature increases, the I_D/I_G values gradually decrease from 0.83 (NGPC/NCNT-800) to 0.75 (NGPC/NCNT-900) to 0.66 (NGPC/NCNT-1000), which are significantly lower than that of NPC (1.04). Moreover, the appearance of distinct peaks at 2680 cm^{-1} (2D band) and 2900 cm^{-1} (D+G band) in Raman spectrum of NGPC/NCNT-900 further confirms the presence of highly graphitized nanostructures with thin walls of few graphitic layers (inset in Figure 3c).^{40, 41} Furthermore, both NGPC/NCNTs and NPC show higher I_D/I_G values than their nitrogen-undoped counterparts GPC (0.63) and C-MOF-5 (1.01), respectively, indicating the disruption of perfect graphitic lattice of the sp^2 -hybridized carbon caused by nitrogen incorporation.³⁶

The N_2 sorption isotherms of NGPC/NCNTs show similar hybrid I/IV-Type behavior with sharp uptakes at low relative pressure ($P/P_0 < 0.015$) and pronounced hysteresis loop at P/P_0 above 0.45 (Figure S7a), suggesting a hierarchically porous characteristic with pore size distribution (PSD) in a wide range from micropores to macropores, which is testified by their corresponding PSD curves calculated by the nonlocal density functional theory (NL-DFT) model (Figure S7b). The Brunauer–Emmett–Teller (BET) specific surface area (SSA) and total pore volume of NGPC/NCNT-900 are 1053 $\text{m}^2 \text{g}^{-1}$ and 1.05 $\text{cm}^3 \text{g}^{-1}$ (> 80% are meso/macropores), respectively, which are comparable to those of NPC (1157 $\text{m}^2 \text{g}^{-1}$ and 1.24 $\text{cm}^3 \text{g}^{-1}$), but higher than those of NGPC/NCNT-800 (962 $\text{m}^2 \text{g}^{-1}$ and 1.01 $\text{cm}^3 \text{g}^{-1}$) and NGPC/NCNT-1000 (961 $\text{m}^2 \text{g}^{-1}$ and

0.99 cm³ g⁻¹). For comparison, the sorption isotherms of MOF-5, C-MOF-5 and GPC are also presented (Figure S7), and the pore characteristics are displayed in Table S2. Interestingly, in addition to similar sorption behavior, all carbon samples exhibit almost the same peak diameters (0.68, 1.30 and 1.48 nm) in the micropore region of their PSD curves, which are the same as those of MOF-5 (Figure S8). Undoubtedly, the prearranged distribution of organic units in highly regular MOF structures is responsible for the inherited intrinsic atomic arrangements of carbon materials after carbonization, no matter the catalytic graphitization proceeds or not. Notably, besides the catalytic role, Ni NPs can also be deemed as a template for the formation of meso/macropore after their removal by hydrothermal etching, as evidenced by TEM images of GPCs shown in Figure S9. This can significantly offset the shrinkage of the porosity caused by graphitization, thus maintaining decent SSA (559 m² g⁻¹) and total pore volume (0.71 cm³ g⁻¹) for GPCs.

Gleaning the above results altogether, we can propose an explicit understanding toward the stepwise structural evolution from MOF-5 to NGPC/NCNTs, and justify the optimization and superiority of our synthetic route. Firstly, the primary carbide C₅₅₀, rather than the moisture-sensitive MOF-5, was elaborately chosen as the host matrix for impregnation of nickel salts, not only because C₅₅₀ is more suitable for post-handling, but also it is more effective in the formation of GPCs with higher yields. Since ZnO in situ generated from thermal decomposition of MOF-5 could oxidize carbon atoms, and also may suppress the generation of metallic Ni catalysts due to the formation of Ni₃ZnC_{0.7} and NiZn alloy at 550 °C and 800 °C, respectively (Figure S10–11).⁴² In addition, C₅₅₀ with ZnO being exiled features a SSA of 1316 m² g⁻¹ (Figure S12 and Table S2), which is twice more than that of MOF-5 (541 m² g⁻¹), thus can facilitate a more effective catalytic graphitization. Moreover, the pre-anneal of MOF-5 was conducted at 550 °C, where the framework of MOF-5 totally collapsed and the carbonization just began, as depicted in thermogravimetric (TG) curve of MOF-5 (Figure S13). This endows C₅₅₀ with abundant oxygen-containing groups to effectively anchor and reduce Ni(II) salts at relative low temperature, resulting in an enhanced catalytic graphitization when compared with the carbides obtained at higher temperatures (Figure S14–16).²⁷ Furthermore, the simultaneous introduction of Ni(II) salts and urea into C₅₅₀ could result in a low nitrogen content (1.83 wt%) in the resultant DCs, which is less than half of that when only urea was added, although a better-crystallized graphitic structure was obtained (Figure S17). And even when double-dose of urea was used when other conditions kept the same, only a slight increase of nitrogen content (2.50 wt%) was obtained. These are plausibly attributed to the different grafting affinities of Ni²⁺ and urea with the oxygen-containing groups on the surface of C₅₅₀, ending up with a competitive result of more reduction of Ni²⁺ than incorporation of the nitrogen. Herewith, a sequential addition of Ni(II) salts and urea in two separate steps was adopted. The role played by Ni NPs in the catalytic graphitization of raw carbon is mainly considered to be a transport by dissolution and re-precipitation of carbon atoms with NiC_x as the intermediates at temperatures above 800 °C,⁴³ therefore, the amorphous C₅₅₀ around them can be successively transformed into highly graphitized GPCs. In order to gain a rich nitrogen doping, majority of Ni species were eliminated by rigorous hydrothermal etching after the

catalytic graphitization was completed, resulting in many hollow onion-like carbons in GPCs. Prior to the following nitrogen doping, GPCs were further rinsed in HNO₃ solution for regenerating oxygen-containing groups on their surfaces to react with urea. The direct nitridation of GPCs generated NGPCs, whose irregular shape results from the breakage of MOF-5 microplates during carbonization, since the integrity of a big-size MOF is more vulnerable at high temperature than a small one.⁴⁴ Notably, the evolution of NCNTs in NGPC/NCNTs is attributed to the repeated dissolve-precipitate behavior of carbon nitride species (e.g., C₂N₂⁺, C₃N₂⁺, C₃N₃⁺) generated from the decomposition of urea on the surface of the residual Ni NPs in GPCs.⁴⁵⁻⁴⁷ It should be mentioned that urea as a cheap and high nitrogen content (46 wt%) compound can not only act as the carbon and nitrogen suppliers for catalytic growth of NCNTs, but also as expansion agent and etchant to recover high SSAs of NGPC/NCNTs from GPCs due to the gases (e.g., NH₃ and (CN)₂) explosively released during its decomposition.⁴⁸ Since there is a trace amount of Ni NPs in GPCs, the presence of NCNTs is not dominated in NGPC/NCNTs. However, the yield of NCNTs at 900 °C is obviously higher than the other two temperatures as investigated by SEM and TEM (Figure 2, S1 and S2), which can be potentially ascribed to that the driving force for growth of NCNTs is insufficient when the nitridation is performed at 800 °C, while the nitrogen content will be quickly diminished at 1000 °C. As a result, 900 °C is the most suitable temperature for the growth of NCNTs under current experimental conditions. The more NCNTs in the hybrids, the higher the electronic conductivity,²³ which combines with the rich nitrogen doping and high SSA, making NGPC/NCNT-900 the optimal catalyst among them (vide infra). Compared with traditional approaches for the synthesis of NCNTs (e.g., CVD or arc process), this in situ synthetic method developed in present work is a new and more cost-effective route. Although NCNTs have been prepared straightforwardly from Zn-Fe-ZIF and show high ORR activities, the originally N-coordinated Fe atoms in Zn-Fe-ZIF have played a pivotal role in both the formation of nanotubes and ORR active sites.⁴⁹ Thus it is not general in synthesis. Apparently, our synthetic strategy may be applied to a wide range of MOF materials, which will provide new insight into the synthesis of more active carbon-based ORR catalysts derived from MOFs.

Activities and Durability of Electrocatalysts

To evaluate the ORR activities of NGPC/NCNTs, cyclic voltammetry (CV) measurement was initially performed. For comparison, NPC, GPC, C-MOF-5 and a commercial Pt/C (20 wt% Pt on Vulcan carbon black, Johnson Matthey) were also tested under identical conditions. As shown in Figure 4a and S18, the CV profiles for all samples exhibit negligible redox features and well-defined cathodic peaks in N₂- and O₂-saturated solutions, respectively, implying that these catalysts are ORR active. Impressively, NGPC/NCNT-900 stands out from these samples with the most positive ORR peak potential (-161 mV) and the largest cathodic current density (0.68 mA cm⁻²), which are slightly higher than those of Pt/C (-163 mV and 0.60 mA cm⁻²). RDE measurement was then used to further probe the ORR activities of different catalysts (Figure 4b). Generally, all carbon samples give comparable current densities from 4.5 to 5.1 mA cm⁻² at -1.0 V. However, the nitrogen-undoped samples exhibit very poor

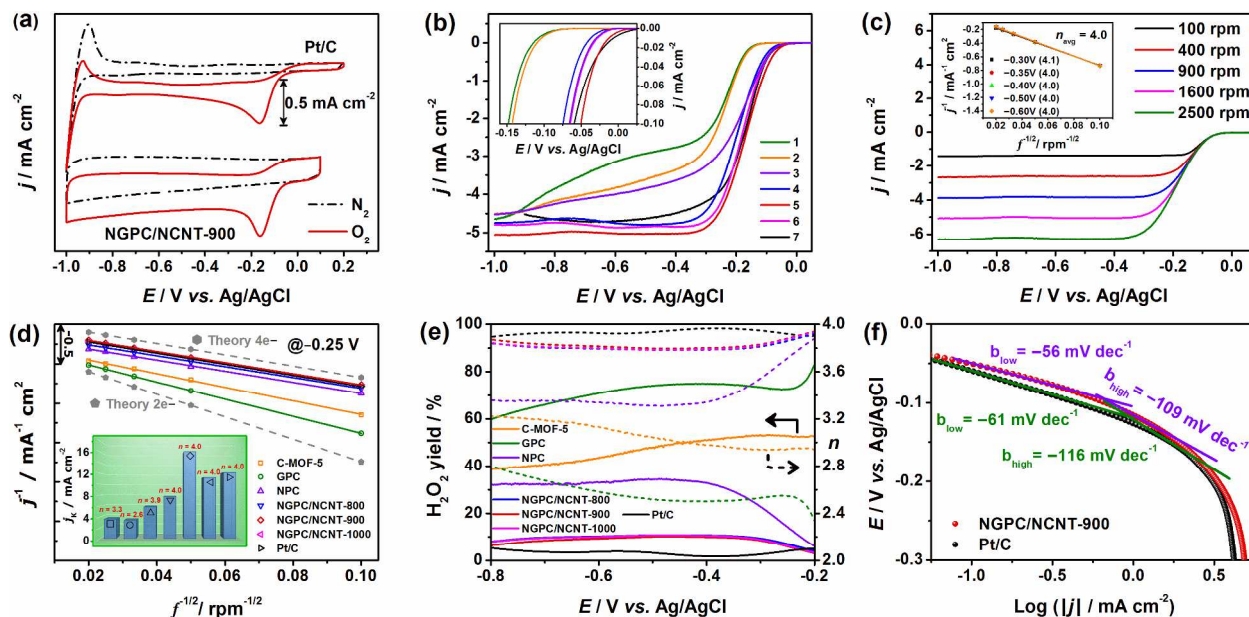


Figure 4. (a) Comparative CVs of NGPC/NCNT-900 and Pt/C; (b) LSVs of GPC (1), C-MOF-5 (2), NPC (3), NGPC/NCNT-800 (4), NGPC/NCNT-900 (5), NGPC/NCNT-1000 (6) and Pt/C (7) in O₂-saturated 0.1 M KOH with a sweep rate of 5 mV s⁻¹ and electrode rotation speed of 1600 rpm, inset: magnification of the potential region of the ORR onset; (c) LSVs of NGPC/NCNT-900 at different rotation speeds (inset shows the corresponding K–L plots at selected potentials); (d) Comparative K–L plots and kinetic current densities (j_k , inset) for all samples at -0.25 V; (e) H₂O₂ yield (solid, primary Y-axis) and the corresponding electron transfer number (n , dashed, second Y-axis) of different samples; (f) Tafel plots for NGPC/NCNT-900 and Pt/C extracted from (b).

ORR activities in terms of E_0 (defined as the potential where the cathodic reduction current density of 0.1 mA cm⁻² is reached, see inset in Figure 4b) and $E_{1/2}$,⁴⁴ the values are -143 and -263 mV for C-MOF-5 and -148 and -292 mV for GPC, respectively. Obviously, the activities of the nitrogen-doped samples are greatly improved (Table S1). NGPC/NCNT-900 harvests the largest j_L value with slightly more positive values in E_0 (-51 mV) and $E_{1/2}$ (-171 mV) than those of Pt/C (-59 mV in E_0 and -172 mV in $E_{1/2}$), further confirming its highest ORR activity. In contrast, both NGPC/NCNT-800 and NGPC/NCNT-1000 show relatively inferior ORR activities, but their current densities can still surpass that of Pt/C at potentials below -0.25 and -0.20 V, respectively. As for NPC, although it holds an E_0 value (-66 mV) close to those of NGPC/NCNTs, a relatively low $E_{1/2}$ value (-205 mV) is observed. In the acidic electrolyte, the activity of NGPC/NCNT-900 is to some extent lower than that of Pt/C, but not too far behind it (ca. $\Delta E_{1/2} = 100$ mV), and is 80 mV higher in $E_{1/2}$ than that of NPC (Figure S19).

In order to get deep insights into ORR mechanism involving the carbon samples, linear-sweep voltammeteries (LSVs) on rotating disk electrode (RDE) were recorded at rotation speeds from 100 to 2500 rpm, accompanied by the corresponding Koutecky–Levich (K–L) plots and electron transfer numbers (n) per oxygen molecule calculated at various potentials (Figure 4c and S20). The LSVs of NGPC/NCNT-900 show relatively wide plateaus of currents below -0.3 V at all rotational speeds, indicating a diffusion-controlled process with an efficient one-step four-electron ($4e^-$) dominant ORR pathway,²² which is further confirmed by its almost identical K–L plots in the potential range from -0.3 to -0.6 V (inset in Figure 4c). The linearity of each plot for NGPC/NCNT-900 suggests its first-order reaction kinetics with regard to the concentration of dissolved oxygen. The K–L plots of all

samples at -0.25 V are presented in Figure 4d. The highly parallelism of the plots of NGPC/NCNTs and NPC to the line representing for theoretical $4e^-$ transfer indicates their n values approach 4.0, as is the case for Pt/C catalyst. Whereas, the plots of C-MOF-5 and GPC deviate from the line representing for theoretical $4e^-$ transfer to some extent with n values of 3.3 and 2.6, respectively, indicating a combined $2e^-$ and $4e^-$ ORR pathway. The kinetic current densities (j_k) at -0.25 V for all samples are then calculated from their corresponding K–L plots, and the results are graphed in inset of Figure 4d. The j_k values of NGPC/NCNTs are markedly higher than those of NPC, GPC and C-MOF-5. Most impressively, NGPC/NCNT-900 gains the largest j_k value (16.07 mA cm⁻²), which reaches 1.3 and 2.75 times more than that of Pt/C (12.18 mA cm⁻²) and NPC (5.84 mA cm⁻²), respectively, highlighting its fast kinetics for ORR in the alkaline medium.

The rotating ring-disk electrode (RRDE) technique was used to further verify ORR pathway by monitoring the formation of intermediate peroxide species during ORR process (Figure 4e). Remarkably, the ORR on NGPC/NCNTs yields about 3.04–10.8% H₂O₂ over a wide potential range from -0.2 to -0.8 V with n ranging from 3.78 to 3.94, suggesting their ORR process favors a high selectivity of OH⁻ as the main product.⁵⁰ In contrast, NPC, C-MOF-5 and GPC give much higher amounts of H₂O₂ under identical conditions, their average H₂O₂ yields and n values are 29.2% (3.41), 46.9% (3.06) and 71.3% (2.57), respectively, which are inferior to those of NGPC/NCNTs. These results are in accordance with the RDE measurements, indicating the highest electrocatalytic efficiency of NGPC/NCNT-900.

The mechanistic and kinetic differences of catalytic ORR between NGPC/NCNT-900 and Pt/C were further evaluated using Tafel plots (Figure 4f).⁵¹ Both of the plots show typical two-stage linear regions in low and high current density ranges

from -1.2 to -0.7 and from 0 to 0.25 on the log scale, respectively, manifesting NGPC/NCNT-900 experienced a same switch from Temkin to Langmuir adsorption mechanism of oxygen as that on Pt surface during ORR.⁵² The Tafel slopes of NGPC/NCNT-900 in the two regions are similar to those of Pt/C (56 vs. 61 and 109 vs. 116 , mV dec^{-1} , respectively), which is in agreement with their similar electron transfer numbers. Since a lower value of the Tafel slope implies faster kinetics as it permits a faster attainment of higher catalytic current density under lower applied potential, therefore endowing NGPC/NCNT-900 a better kinetic property than Pt/C. To our knowledge, the ORR activity of NGPC/NCNT-900 also outperforms most of non-noble metal catalysts and ranks among the best carbon-based catalysts derived from MOFs in an alkaline medium (see Table S3).

To authenticate the factors that influence on ORR activities of the catalysts, we take a brief discussion as follows. Obviously, the significantly boosted ORR activities of DCs over their raw counterparts (C-MOF-5 and GPC) clearly exemplify the negligible contribution of Ni residues and the critical role of nitrogen dopants.⁵³ However, the decreased nitrogen content in NGPC/NCNTs does not lead to a commensurate drop in ORR activity, indicating the ORR activity is more correlated to the content of certain specific N species. It is claimed that the pyridinic-N and pyrrolic-N located at graphitic plane sites should be responsible for high ORR activity, especially high E_0 value, while the graphitic-N at the zigzag graphene edges contributes more for high j_L value.^{36, 54, 55} As shown in Table S1, NPC has the largest content of pyridinic-N and pyrrolic-N (N1+N2, 5.52 wt%), thus exhibiting an E_0 value on a par with NGPC/NCNT-1000, which is 10 mV more positive than that of NGPC/NCNT-800. And the j_L values of NGPC/NCNTs respond well to their variation in content of graphitic-N. It should be mentioned that the nitrogen dopant is not the solely conclusive factor, the high graphitic degree (more rapid electron transfer rate) and high SSA (more exposed active sites and accessible surface area for mass transport, i.e., O_2 and electrolyte) are also believed to synergistically exert great influence on the ORR activity, justified by the highest E_0 and j_L values of NGPC/NCNT-900 with moderate contents of nitrogen. It can be anticipated that the performance of NGPC/NCNT-900 may be further improved using an optimized nitrogen doping and/or a more porous MOF precursor.

Since ORR catalysts should be robust in real application system, the durability and the tolerance toward methanol crossover of NGPC/NCNT-900 were further examined by using current-time ($i-t$) chronoamperometry technology at constant cathodic voltage of -0.2 and -0.3 V in O_2 -saturated electrolyte, respectively. For comparison, the activity of Pt/C was also measured in the same way. As shown in Figure 5a, the accelerated durability of both catalysts were tested for 12 h. A high relative current of 86% still persists for NGPC/NCNT-900, while Pt/C maintains only 67% of its initial activity over the same time period. Obviously, the much slower decay in current of NGPC/NCNT-900 is a synergistic contribution arising from its highly graphitized carbon skeletons and the actual active sites caused by nitrogen doping, thereby can reinforce its corrosion resistance and avoid the detachment of active sites from the hosts during continuous chronoamperometric measurements. Moreover, the $i-t$ chronoamperometric responses to O_2 -saturated electrolyte

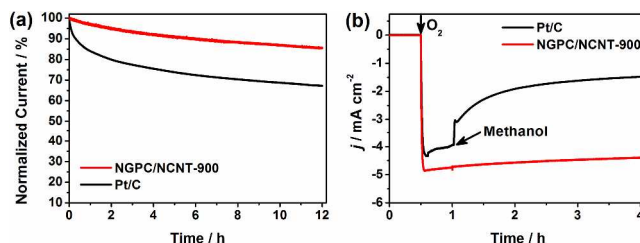


Figure 5. (a) Current-time ($i-t$) chronoamperometric responses of NGPC/NCNT-900 and Pt/C electrodes (1600 rpm) at -0.2 V in O_2 -saturated 0.1 M KOH solution. (b) Current-time ($i-t$) chronoamperometric responses of NGPC/NCNT-900 and Pt/C electrodes (1600 rpm) at -0.3 V in N_2 -saturated 0.1 M KOH solution followed by the introduction of O_2 and methanol (3 M).

(125 mL) in the presence of 3 M methanol were conducted (Figure 5b). After the methanol injection, a dramatic drop up to more than 25% of the initial current is observed for Pt/C, and an overall current loss of nearly 63% occurs after 3 h. Whereas no noticeable response is detected under the same conditions for NGPC/NCNT-900, indicating the inertness of NGPC/NCNT-900 to methanol electrooxidation. This obvious difference in response to methanol is further evidenced by their CVs and LSVs (Figure S21). The excellent selectivity of NGPC/NCNT-900 toward ORR is probably attributed to its chemical expectations unlike that of Pt/C, which endows it a much lower potential for ORR than that required for electrooxidation of methanol, finally evading the current attenuation caused by the mixed potential. These results unambiguously disclose that NGPC/NCNT-900 possesses better long-term durability, higher selectivity and stronger immunity toward methanol crossover than Pt/C, which makes it highly promising as a Pt-substituted ORR electrocatalyst for practical applications.

CONCLUSIONS

We have developed an attractive route for the synthesis of highly graphitized NGPC/NCNT hybrids from MOF-5 with a successive carbonization, catalytic graphitization and nitridation process. The stepwise structural evolution from MOF-5 to NGPC/NCNTs has been studied in detail, which is expected to be generalized to a broad variety of MOF materials. Compared with the nitrogen-doped porous carbons straightforwardly prepared from pristine MOF-5, NGPC/NCNTs show much enhanced degree of graphitization but comparable high surface areas, moreover, NGPC/NCNTs possess unique heterostructure to form the interconnected 3D conductive network through NCNTs bridging dissociative NGPCs, thereby demonstrating superior ORR activities. The electroactivity (especially the $E_{1/2}$ value), cycling durability and methanol tolerance of NGPC/NCNT-900 have out-competed those of the commercial Pt/C benchmark, which ranks it one of the best ORR electrocatalysts derived from MOFs. In summary, this study not only shows that NGPC/NCNT-900 may serve as a promising alternative to Pt-based ORR catalysts in alkaline fuel cells, but also opens up new possibilities for the synthesis of a variety of more active carbon-based ORR catalysts derived from MOFs.

ASSOCIATED CONTENT

Supporting Information

Additional SEM and TEM images, XPS and Raman spectra, PXRD patterns, TGA curve, FT-IR spectra and N₂-physisorption data of the hierarchically porous carbons. Electrochemical data, i.e., cyclic voltammograms, polarization curves and K–L plots of different samples. This material is available free of charge via the Internet at <http://pubs.acs.org>.

AUTHOR INFORMATION

Corresponding Author

*Address correspondence to: ruihu@fjirsm.ac.cn (R. Wang)

Notes

The authors declare no competing financial interest.

ACKNOWLEDGMENT

This work was financially supported by the 973 Program (2011CBA00502) and the Natural Science Foundation (21273239 and 21471151) of China.

REFERENCES

- (1) Cao, R.; Lee, J.-S.; Liu, M.; Cho, J. Recent Progress in Non-Precious Catalysts for Metal-Air Batteries. *Adv. Energy Mater.* **2012**, *2*, 816-829.
- (2) Li, Q.; Cao, R.; Cho, J.; Wu, G. Nanocarbon Electrocatalysts for Oxygen Reduction in Alkaline Media for Advanced Energy Conversion and Storage. *Adv. Energy Mater.* **2014**, *4*, 1301415.
- (3) Nie, Y.; Li, L.; Wei, Z. Recent Advancements in Pt and Pt-free Catalysts for Oxygen Reduction Reaction. *Chem. Soc. Rev.* **2015**, *44*, 2168-2201.
- (4) Jin, J.; Pan, F.; Jiang, L.; Fu, X.; Liang, A.; Wei, Z.; Zhang, J.; Sun, G. Catalyst-Free Synthesis of Crumpled Boron and Nitrogen Co-Doped Graphite Layers with Tunable Bond Structure for Oxygen Reduction Reaction. *ACS Nano* **2014**, *8*, 3313-3321.
- (5) Paraknowitsch, J. P.; Thomas, A. Doping Carbons beyond Nitrogen: an Overview of Advanced Heteroatom Doped Carbons with Boron, Sulphur and Phosphorus for Energy Applications. *Energy Environ. Sci.* **2013**, *6*, 2839-2855.
- (6) Liang, H.-W.; Wei, W.; Wu, Z.-S.; Feng, X.; Müllen, K. Mesoporous Metal–Nitrogen-Doped Carbon Electrocatalysts for Highly Efficient Oxygen Reduction Reaction. *J. Am. Chem. Soc.* **2013**, *135*, 16002-16005.
- (7) Qu, L.; Liu, Y.; Baek, J.-B.; Dai, L. Nitrogen-Doped Graphene as Efficient Metal-Free Electrocatalyst for Oxygen Reduction in Fuel Cells. *ACS Nano* **2010**, *4*, 1321-1326.
- (8) Nam, G.; Park, J.; Kim, S. T.; Shin, D.-b.; Park, N.; Kim, Y.; Lee, J.-S.; Cho, J. Metal-Free Ketjenblack Incorporated Nitrogen-Doped Carbon Sheets Derived from Gelatin as Oxygen Reduction Catalysts. *Nano Lett.* **2014**, *14*, 1870-1876.
- (9) Chaikittisilp, W.; Ariga, K.; Yamauchi, Y. A New Family of Carbon Materials: Synthesis of MOF-Derived Nanoporous Carbons and Their Promising Applications. *J. Mater. Chem. A* **2013**, *1*, 14-19.
- (10) Liu, B.; Shioyama, H.; Akita, T.; Xu, Q. Metal-Organic Framework as a Template for Porous Carbon Synthesis. *J. Am. Chem. Soc.* **2008**, *130*, 5390-5391.
- (11) Zhang, L.; Su, Z.; Jiang, F.; Yang, L.; Qian, J.; Zhou, Y.; Li, W.; Hong, M. Highly Graphitized Nitrogen-Doped Porous Carbon Nanopolyhedra Derived from ZIF-8 Nanocrystals as Efficient Electrocatalysts for Oxygen Reduction Reactions. *Nanoscale* **2014**, *6*, 6590-6602.
- (12) Zhang, P.; Sun, F.; Xiang, Z.; Shen, Z.; Yun, J.; Cao, D. ZIF-derived in Situ Nitrogen-Doped Porous Carbons as Efficient Metal-free Electrocatalysts for Oxygen Reduction Reaction. *Energy Environ. Sci.* **2014**, *7*, 442-450.
- (13) Li, J.; Chen, Y.; Tang, Y.; Dong, H.; Li, K.; Li, S.; Han, M.; Lan, Y.; Bao, J.; Dai, Z. Metal-Organic Frameworks Templated Nitrogen and Sulfur Co-Doped Porous Carbons as Highly Efficient Metal-Free Electrocatalysts for Oxygen Reduction Reaction. *J. Mater. Chem. A* **2014**, *2*, 6316-6319.
- (14) Aijaz, A.; Akita, T.; Yang, H.; Xu, Q. From Ionic-Liquid@Metal-Organic Framework Composites to Heteroatom-Decorated Large-Surface area Carbons: Superior CO₂ and H₂ Uptake. *Chem. Commun.* **2014**, *50*, 6498-6501.
- (15) Wang, X.; Zhou, J.; Fu, H.; Li, W.; Fan, X.; Xin, G.; Zheng, J.; Li, X. MOF Derived Catalysts for Electrochemical Oxygen Reduction. *J. Mater. Chem. A* **2014**, *2*, 14064-14070.
- (16) Xia, W.; Zhu, J.; Guo, W.; An, L.; Xia, D.; Zou, R. Well-Defined Carbon Polyhedrons Prepared from Nano Metal-Organic Frameworks for Oxygen Reduction. *J. Mater. Chem. A* **2014**, *2*, 11606-11613.
- (17) Palaniselvam, T.; Biswal, B. P.; Banerjee, R.; Kurungot, S. Zeolitic Imidazolate Framework (ZIF)-Derived, Hollow-Core, Nitrogen-Doped Carbon Nanostructures for Oxygen-Reduction Reactions in PEFCs. *Chem.-Eur. J.* **2013**, *19*, 9335-9342.
- (18) Li, J.; Li, S.; Tang, Y.; Li, K.; Zhou, L.; Kong, N.; Lan, Y.-Q.; Bao, J.; Dai, Z. Heteroatoms Ternary-Doped Porous Carbons Derived from MOFs as Metal-Free Electrocatalysts for Oxygen Reduction Reaction. *Sci. Rep.* **2014**, *4*, 5130.
- (19) Gong, K.; Du, F.; Xia, Z.; Durstock, M.; Dai, L. Nitrogen-Doped Carbon Nanotube Arrays with High Electrocatalytic Activity for Oxygen Reduction. *Science* **2009**, *323*, 760-764.
- (20) Ding, W.; Wei, Z.; Chen, S.; Qi, X.; Yang, T.; Hu, J.; Wang, D.; Wan, L.-J.; Alvi, S. F.; Li, L. Space-Confinement-Induced Synthesis of Pyridinic- and Pyrrolic-Nitrogen-Doped Graphene for the Catalysis of Oxygen Reduction. *Angew. Chem., Int. Ed.* **2013**, *52*, 11755-11759.
- (21) Sun, X.; Song, P.; Zhang, Y.; Liu, C.; Xu, W.; Xing, W. A Class of High Performance Metal-Free Oxygen Reduction Electrocatalysts based on Cheap Carbon Blacks. *Sci. Rep.* **2013**, *3*, 2505.
- (22) Zhong, H.; Wang, J.; Zhang, Y.; Xu, W.; Xing, W.; Xu, D.; Zhang, Y.; Zhang, X. ZIF-8 Derived Graphene-Based Nitrogen-Doped Porous Carbon Sheets as Highly Efficient and Durable Oxygen Reduction Electrocatalysts. *Angew. Chem., Int. Ed.* **2014**, *53*, 14235-14239.
- (23) Ge, L.; Yang, Y.; Wang, L.; Zhou, W.; De Marco, R.; Chen, Z.; Zou, J.; Zhu, Z. High Activity Electrocatalysts from Metal–Organic Framework–Carbon Nanotube Templates for the Oxygen Reduction Reaction. *Carbon* **2015**, *82*, 417-424.
- (24) Jiang, H. L.; Liu, B.; Lan, Y. Q.; Kuratani, K.; Akita, T.; Shioyama, H.; Zong, F.; Xu, Q. From Metal-organic Framework to Nanoporous Carbon: Toward a Very High Surface Area and Hydrogen Uptake. *J. Am. Chem. Soc.* **2011**, *133*, 11854-11857.
- (25) Radhakrishnan, L.; Reboul, J.; Furukawa, S.; Srinivasu, P.; Kitagawa, S.; Yamauchi, Y. Preparation of Microporous Carbon Fibers through Carbonization of Al-Based Porous Coordination Polymer (Al-PCP) with Furfuryl Alcohol. *Chem. Mater.* **2011**, *23*, 1225-1231.
- (26) Ma, T. Y.; Dai, S.; Jaroniec, M.; Qiao, S. Z. Metal–Organic Framework Derived Hybrid Co₃O₄-Carbon Porous Nanowire Arrays as Reversible Oxygen Evolution Electrodes. *J. Am. Chem. Soc.* **2014**, *136*, 13925-13931.
- (27) Sevilla, M.; Fuertes, A. B. Catalytic Graphitization of Templated Mesoporous Carbons. *Carbon* **2006**, *44*, 468-474.
- (28) Krivoruchko, O. P.; Maksimova, N. I.; Zaikovskii, V. I.; Salanov, A. N. Study of Multiwalled Graphite Nanotubes and Filaments Formation from Carbonized Products of Polyvinyl Alcohol via Catalytic Graphitization at 600–800 °C in Nitrogen Atmosphere. *Carbon* **2000**, *38*, 1075-1082.
- (29) Su, P.; Jiang, L.; Zhao, J.; Yan, J.; Li, C.; Yang, Q. Mesoporous Graphitic Carbon Nanodisks Fabricated via Catalytic Carbonization of Coordination Polymers. *Chem. Commun.* **2012**, *48*, 8769-8771.
- (30) Zhang, L.; Hu, Y. H. A Systematic Investigation of Decomposition of Nano Zn₄O(C₈H₄O₄)₃ Metal–Organic Framework. *J. Phys. Chem. C* **2010**, *114*, 2566-2572.
- (31) Zhou, R.; Qiao, S. Z. An Fe/N Co-Doped Graphitic Carbon Bulb for High-Performance Oxygen Reduction Reaction. *Chem. Commun.* **2015**, *51*, 7516-7519.

- (32) Chung, H. T.; Won, J. H.; Zelenay, P. Active and Stable Carbon Nanotube/Nanoparticle Composite Electrocatalyst for Oxygen Reduction. *Nat. Commun.* **2013**, *4*, 1922.
- (33) Zhang, W.; Wu, Z.-Y.; Jiang, H.-L.; Yu, S.-H. Nanowire-Directed Templating Synthesis of Metal–Organic Framework Nanofibers and Their Derived Porous Doped Carbon Nanofibers for Enhanced Electrocatalysis. *J. Am. Chem. Soc.* **2014**, *136*, 14385-14388.
- (34) Nagaiah, T. C.; Bordoloi, A.; Sánchez, M. D.; Muhler, M.; Schuhmann, W. Mesoporous Nitrogen-Rich Carbon Materials as Catalysts for the Oxygen Reduction Reaction in Alkaline Solution. *ChemSusChem* **2012**, *5*, 637-641.
- (35) Stańczyk, K.; Dziembaj, R.; Piwowarska, Z.; Witkowski, S. Transformation of Nitrogen Structures in Carbonization of Model Compounds Determined by XPS. *Carbon* **1995**, *33*, 1383-1392.
- (36) Cong, H.-P.; Wang, P.; Gong, M.; Yu, S.-H. Facile Synthesis of Mesoporous Nitrogen-Doped Graphene: An Efficient Methanol-Tolerant Cathodic Catalyst for Oxygen Reduction Reaction. *Nano Energy* **2014**, *3*, 55-63.
- (37) Liu, X.; Zhou, L.; Zhao, Y.; Bian, L.; Feng, X.; Pu, Q. Hollow, Spherical Nitrogen-Rich Porous Carbon Shells Obtained from a Porous Organic Framework for the Supercapacitor. *ACS Appl. Mater. Interfaces* **2013**, *5*, 10280-10287.
- (38) Liang, J.; Zhou, R. F.; Chen, X. M.; Tang, Y. H.; Qiao, S. Z. Fe–N Decorated Hybrids of CNTs Grown on Hierarchically Porous Carbon for High-Performance Oxygen Reduction. *Adv. Mater.* **2014**, *26*, 6074-6079.
- (39) Sadezky, A.; Muckenhuber, H.; Grothe, H.; Niessner, R.; Pöschl, U. Raman Microspectroscopy of Soot and Related Carbonaceous Materials: Spectral Analysis and Structural Information. *Carbon* **2005**, *43*, 1731-1742.
- (40) Ferrari, A. C.; Basko, D. M. Raman Spectroscopy as a Versatile Tool for Studying the Properties of Graphene. *Nat. Nanotechnol.* **2013**, *8*, 235-246.
- (41) Duan, J.; Chen, S.; Dai, S.; Qiao, S. Z. Shape Control of Mn₃O₄ Nanoparticles on Nitrogen-Doped Graphene for Enhanced Oxygen Reduction Activity. *Adv. Funct. Mater.* **2014**, *24*, 2072-2078.
- (42) Kong, A.; Lin, Q.; Mao, C.; Bu, X.; Feng, P. Efficient Oxygen Reduction by Nanocomposites of Heterometallic Carbide and Nitrogen-Enriched Carbon Derived from the Cobalt-Encapsulated Indium-MOF. *Chem. Commun.* **2014**, *50*, 15619-15622.
- (43) Marsh, H.; Warburton, A. P. Catalysis of Graphitisation. *J. Appl. Chem.* **1970**, *20*, 133-142.
- (44) Zhao, S.; Yin, H.; Du, L.; He, L.; Zhao, K.; Chang, L.; Yin, G.; Zhao, H.; Liu, S.; Tang, Z. Carbonized Nanoscale Metal–Organic Frameworks as High Performance Electrocatalyst for Oxygen Reduction Reaction. *ACS Nano* **2014**, *8*, 12660-12668.
- (45) Gao, S.; Li, G.-D.; Liu, Y.; Chen, H.; Feng, L.-L.; Wang, Y.; Yang, M.; Wang, D.; Wang, S.; Zou, X. Electrocatalytic H₂ Production from Seawater over Co, N-Codoped Nanocarbons. *Nanoscale* **2015**, *7*, 2306-2316.
- (46) Su, Q.; Sun, J.; Wang, J.; Yang, Z.; Cheng, W.; Zhang, S. Urea-Derived Graphitic Carbon Nitride as an Efficient Heterogeneous Catalyst for CO₂ Conversion into Cyclic Carbonates. *Catal. Sci. Technol.* **2014**, *4*, 1556-1562.
- (47) Wen, Z.; Ci, S.; Hou, Y.; Chen, J. Facile One-Pot, One-Step Synthesis of a Carbon Nanoarchitecture for an Advanced Multifunctional Electrocatalyst. *Angew. Chem., Int. Ed.* **2014**, *53*, 6496-6500.
- (48) Wakeland, S.; Martinez, R.; Grey, J. K.; Luhrs, C. C. Production of Graphene from Graphite Oxide Using Urea as Expansion-Reduction Agent. *Carbon* **2010**, *48*, 3463-3470.
- (49) Su, P.; Xiao, H.; Zhao, J.; Yao, Y.; Shao, Z.; Li, C.; Yang, Q. Nitrogen-Doped Carbon Nanotubes Derived from Zn-Fe-ZIF Nanospheres and Their Application as Efficient Oxygen Reduction Electrocatalysts with in situ Generated Iron Species. *Chem. Sci.* **2013**, *4*, 2941-2946.
- (50) Zhou, R.; Qiao, S. Z. Silver/Nitrogen-Doped Graphene Interaction and Its Effect on Electrocatalytic Oxygen Reduction. *Chem. Mater.* **2014**, *26*, 5868-5873.
- (51) Jiao, Y.; Zheng, Y.; Jaroniec, M.; Qiao, S. Z. Design of Electrocatalysts for Oxygen- and Hydrogen-Involving Energy Conversion Reactions. *Chem. Soc. Rev.* **2015**, *44*, 2060-2086.
- (52) Ma, G.; Jia, R.; Zhao, J.; Wang, Z.; Song, C.; Jia, S.; Zhu, Z. Nitrogen-Doped Hollow Carbon Nanoparticles with Excellent Oxygen Reduction Performances and Their Electrocatalytic Kinetics. *J. Phys. Chem. C* **2011**, *115*, 25148-25154.
- (53) Kattel, S.; Wang, G. A Density Functional Theory Study of Oxygen Reduction Reaction on Me-N₄ (Me = Fe, Co, or Ni) Clusters between Graphitic Pores. *J. Mater. Chem. A* **2013**, *1*, 10790-10797.
- (54) Lai, L.; Potts, J. R.; Zhan, D.; Wang, L.; Poh, C. K.; Tang, C.; Gong, H.; Shen, Z.; Lin, J.; Ruoff, R. S. Exploration of the Active Center Structure of Nitrogen-Doped Graphene-Based Catalysts for Oxygen Reduction Reaction. *Energy Environ. Sci.* **2012**, *5*, 7936-7942.
- (55) Qu, K.; Zheng, Y.; Dai, S.; Qiao, S. Z. Polydopamine-Graphene Oxide Derived Mesoporous Carbon Nanosheets for Enhanced Oxygen Reduction. *Nanoscale* **2015**, *7*, 12598-12605.

Table of Contents (TOC)

Structural Evolution from Metal-Organic Framework to Hybrids of Nitrogen-Doped Porous Carbon and Carbon Nanotube for Enhanced Oxygen Reduction Activity

Linjie Zhang, Xiuyun Wang, Ruihu Wang* and Maochun Hong

